Effects of Temperature on the Alignment and Electrooptical Responses of a Nematic Nanoscale Liquid Crystalline Film

Lay Min Lee, Hye J. Kwon, Ralph G. Nuzzo,* and Ken S. Schweizer*

Department of Chemistry, Department of Materials Science and Engineering, and the Frederick Seitz Materials Research Laboratory, University of Illinois at Urbana-Champaign, Urbana, Illinois 61801

Received: October 21, 2005; In Final Form: May 1, 2006

The surface-induced alignment and electrooptical (EO) dynamics of a 50-nm-thick liquid crystalline (4-*n*-pentyl-4′-cyanobiphenyl; 5CB) film were studied at three temperatures: 25 and 33 °C (near the crystalline−nematic and nematic−isotropic transition temperatures, respectively) and 29 °C (a median temperature in the stability region of the nematic phase). The ZnSe surfaces that entrap the liquid crystal (LC) film have been polished unidirectionally to produce a grooved surface presenting nanometer-scale corrugations, a structure that induces a planar and homogeneous orientation in the nematic phase. The present work attempts to understand the influences of temperature on the surface-induced alignment and corresponding EO dynamics of the material. Step-scan time-resolved spectroscopy measurements were made to determine the rate constants for the electric-field-induced orientation and thermal relaxation of the 5CB film. The field-driven orientation rates vary sensitively with temperature across a range that spans the stability limits of the nematic phase; the relaxation rates, however, vary very little across this same temperature range. We propose that these differences in LC behavior arise as consequence of the interplay of the temperature dependence of the elastic constants, viscosity, and degree of orientational order of the LC medium. A simple theoretical model provides some understanding of these behaviors.

Introduction

Fundamental understanding of interfacial interactions between fluids and surfaces are important for advancing progress in many areas of technology. In diverse fields such as biomaterials[1] and tribology,[2] for example, substantial influences are known to originate as direct consequences of the molecular structure and compositions present at an interface. These, in turn, provide a rich set of mechanisms through which complex functional properties of a system can be modified (e.g., to promote adhesion[3] or inhibit wear[4]) or controlled (e.g., to inhibit an inflammatory response to a medical prosthetic device[5]).

This report is concerned with a system in which interfacial actions provide a critical control mechanism, one that enables the multibillion dollar commercial technology of flat-panel liquid crystal displays (LCDs).[6] The functioning of these devices and their energy efficiency depends very sensitively on the controlling impacts of anchoring interactions.[7−11] These interactions most typically involve both molecular and more coarse-grained physical contributions as the means for controlling the mesoscopic organization that make it possible to exploit the electrooptical properties of liquid crystalline phases.[12,13]

Much research has been conducted on the effects of surface properties on the alignment of liquid crystalline mesophases,[9,14,15] and the methods through which specific alignments can be induced, whether textured,[16−18] chemical,[19,20] or other,[21,22] are now well established. Even so, the physics of these influences (especially as regards to their impacts on electrooptical dynamics[23−25]) remain incompletely understood, and there exist opportunities to exploit new approaches to alignment that might serve as the foundation of a vastly more energy-efficient display technology.[26]

In a previous report,[27] we examined the surface-dependent anchoring and electrooptical (EO) dynamics of thin liquid crystalline films using Fourier transform infrared (FTIR) spectroscopy and step-scan time-resolved spectroscopy (TRS). The EO dynamics were shown to be very sensitive to variations in the surface morphologies, and an assessment of the underlying mechanisms involved in the EO dynamic variations was provided by a coarse-grained dynamical model.

The current report studies the convolved impacts of the temperature-dependent elastic constants and hydrodynamic viscosity on the EO dynamics of a prototypical LC material. We specifically explore the influence of temperature on the mediating role of the anchoring interactions. The structural organizations of LC mesophases are very sensitive to thermal influences[28,29] due to the temperature-dependent viscoelastic properties of these materials.[30,31] Temperature also impacts EO dynamical behaviors, although it can do so in complex ways involving many forms of mechanistic underpinnings. We explore these issues for the nematic liquid crystal, 4-*n*-pentyl-4′-cyanobiphenyl (5CB),[12,32] based on the same sample cell as used in our previous study[27] where the alignment of the molecules is induced using long-period, shallow-amplitude corrugations. The effects of temperature on the stability of the structural organization and the corresponding EO dynamics that they induce were examined at three temperatures: 25 and 33 °C (near the crystalline−nematic and nematic−isotropic phase transition temperatures, respectively) and 29 °C (a temperature at the midpoint from either phase boundary). The time scales at which the electric-field-induced orientation and thermal relaxations occur proved to be especially interesting. The softening of the elastic constants at higher temperatures leads to predictably

* Authors to whom correspondence should be addressed. Phone: (217) 244-0809. Fax: (217) 244-2278. E-mail: r-nuzzo@uiuc.edu; kschweiz@uiuc.edu.

10.1021/jp056047u CCC: $33.50
Published on Web 07/27/2006

faster electric-field-induced orientation rates; the relaxation rates, however, do not vary markedly with temperature. These striking experimental results are interpreted and accounted for semi-quantitatively using a theoretical framework presented in our previous report.[27]

Experimental Section

The liquid crystal EO cell employed and its means of fabrication have been described in detail in earlier reports.[27,33−35] The cell used in this study adopts the same design rules as described there. The ZnSe windows were polished to produce a nanometer-scale, grooved morphology that serves to align the LC director. These long-period corrugations were generated by polishing the substrate crystals using motions restricted to within a few degrees along one primary axis. Representative atomic force microscopy (AFM) micrographs of the polished surfaces are given in the earlier report.[27]

The methods of assembling the EO cell with 5CB are the same as those described elsewhere.[33,35] The temperature of the liquid crystalline sample was controlled by attaching flexible Kapton resistive heating elements with pressure-sensitive adhesive surfaces (Watlow, St. Louis, MO) onto the stainless steel sample holder. Four heaters were attached, connected in series, and actuated by applying voltage from a programmable power supply. The temperature of the sample was monitored with a Eurotherm programmable temperature controller via a thermocouple attached underneath the bottom ZnSe piece of the liquid crystalline EO cell and interfaced with the power supply. With this setup, we were able to hold the sample temperature to within ± 0.2 °C of the set point during the experiments.

Two kinds of infrared spectroscopic measurements were made. In the first of these, stable voltages (ranging from 1 to 15 V) were applied to an interdigitated electrode array (IDEA) with a direct current (DC) power supply, and infrared spectra of the induced state were recorded with a Bio-Rad (Cambridge, MA) FTS-6000 FTIR spectrometer. The spacing between electrodes is fixed at 15 μm. In the second set of measurements, the step-scan feature of the FTS-6000 spectrometer was utilized to observe the EO dynamics of the liquid crystalline sample by applying transient electrical polarizations and capturing the corresponding spectroscopic states on a sub-millisecond time scale. Details of all spectroscopic measurements are described in our earlier reports[27,33−35] and will not be discussed here.

Results and Qualitative Discussion

The liquid crystalline material 5CB exhibits a prototypical nematic phase that has been studied extensively in the past.[12,32] While representative of the materials finding use in the earliest versions of LCDs, the demands for high performance have led to the introduction of devices that exploit more complex mesogenic structures typically based on multicomponent LC mixtures.[6,36] Even so, 5CB remains a useful model system for studies of LC dynamics. Its responses to surface morphology and chemistry, for example, have been exhaustively studied and its alignment mechanisms on various surfaces are now reasonably well understood.[7−9] Among the various mechanisms used to align this phase, we examine one that was first discovered in the 1940s by Chatelain[37] (and analyzed in the 1970s by Berreman[16,17]). This is a protocol that, in modified form, the flat-panel display industry still utilizes. By rubbing a surface (usually polymeric) unidirectionally, grooves are formed on it;[16,17] additionally, the frictional heat produced in the process can also serve to align the surface segments of molecular substrates (such as polymer) in the direction of the rubbing.[38]

CHART 1: 4-*n*-Pentyl-4′-cyanobiphenyl (5CB) Molecule[a]

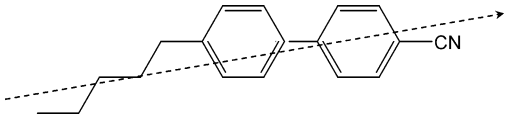

[a] The arrow indicates the approximate optic axis of the molecule.

When a nematic liquid crystalline material such as 5CB is placed on such a surface, the molecules adjacent to the surface preferentially align with their long axis oriented along the length of the grooves to minimize their free energy (via the minimization of elastic strains),[16,17] and these molecules in turn serve to align the bulk material via intermolecular interactions.

Recent work from our group demonstrated that inorganic surfaces such as ZnSe, when treated appropriately, can also effectively manipulate the nematic phase alignment.[34] The present study adopts a recently described refinement of these methods to develop a highly anisotropic planar alignment in 5CB.[27] We adopt here a protocol in which the ZnSe is polished to produce long-period nanometer-scale grooves and study the alignment and dynamics of 5CB induced by it. In particular, we study a specific alignment of the nematic phase that facilitates quantitative comparisons with the predictions of the theoretical model described in our previous work.[27] From past experimental efforts, we expected that the 5CB nematic phase would form a planar structure in the 50-nm-thick EO cell, in which the director aligns in a strongly anisotropic manner along the length of the grooves (and parallel to the electrode digits). The experiments described below confirm this expectation.

1. Polarized IR Responses of 5CB to Static Voltages. Polarized IR spectroscopy was used to determine the organization of the nematic liquid crystalline phase since the IR selection rule yields information about the orientations of molecules present in a sample. The optical polarization of the IR radiation is defined with respect to the IDEA digits as described elsewhere.[27,33−35] The mode assignments for 5CB have been discussed in the literature.[39,40] The structure of 5CB is shown in Chart 1.

The director alignment of the nematic phase is also defined with respect to one (low-energy conformational) representation of the optic axis of the molecule. The orientation of the director is strongly correlated with certain dipole transition moments, such as the ν_{CN} and in-plane aromatic modes, which rigorously lie along the length of the rigid cyanobiphenyl portion of the molecule.[39,40] We focus on the IR modes corresponding to these transition moments as they are both intense and well-resolved in the IR spectra.

Figures 1a−c show the dichroic spectra of 5CB measured at 25, 29, and 33 °C, respectively, a range of temperatures that broadly spans the stability limits of the nematic phase. The modes with transition dipole moments projecting strongly along the optic axis of 5CB, such as the ν_{CN} and in-plane aromatic ring modes, appear as intense positive features in these spectra. The negative intensity features correspond to modes with transition moments lying perpendicular to this axis; these include most notably the out-of-plane ring deformation modes of the aromatic 5CB core. To quantify these data, temperature-dependent dichroic ratios, D, were measured and found to be 2.9 (25 °C), 2.4 (29 °C), and 2.1 (33 °C). Although the full nature of the structural organization of the LC sample cannot be deduced from these data alone, we infer from them that the director of the LC sample exhibits significant in-plane ordering that projects strongly in the parallel direction lying along the length of the electrode digits and the grooves on the ZnSe

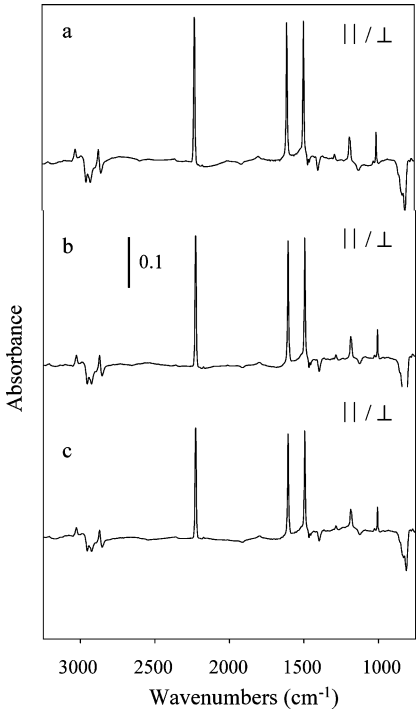

Figure 1. Dichroic spectra of the 5CB film at (a) 25, (b) 29, and (c) 33 °C. The dichroic ratios of these films are 2.9, 2.4, and 2.1, respectively. The positive features in the spectra correspond to the vibrational modes that lie predominantly parallel to the optic axis of 5CB, whereas the negative features are orthogonal to this axis. The spectra indicate that the director of the LC phase lies parallel to the electrode digits.

surface. This alignment, as inferred from the calculated dichroic ratios, increases with cooling as expected.

Representative IR spectra taken during the application of static voltages at 25, 29, and 33 °C over a range of incrementally increased applied voltages (3−15 V or, equivalently, field strengths ranging from 2500 to 10 000 V cm^{-1}) are shown in Figure 2. These data imply that 5CB aligns as expected along the electric-field lines with the magnitude of the field-induced reorganization increasing as stronger fields are applied. The absolute magnitudes of the intensity changes are slightly different for the two infrared polarizations. Those measured in the perpendicular direction are, in absolute measure, weaker than those found in the parallel case. This trend is more fully quantified in Figure 3, in which the voltage-dependent integrated areas for the ν_{CN} mode are plotted; the integrated intensity changes seen with respect to the applied fields also are not exactly commensurate in the two polarizations. One contributor to this difference results from the optics of the IR experiment and the influence of specific projections of transition moments on the measured band intensities.[34] From this voltage-dependent IR data and that of Figure 1, we can develop a general picture of the organization present in the LC sample. In the absence of the applied field, the nematic phase adopts a planar organization in which the director strongly aligns in a collinear fashion along the direction defined by the electrode bands and substrate grooves. This LC organization is one that agrees well with previously published work both from our own group[34] and that of others.[16,17,41−43] The data of Figure 3 also suggest that some minor out-of-plane alignments of 5CB may also be present, a fact that has some impacts on the field-dependent dynamics of the material. We discuss this point in more detail below.

2. Electrooptical Dynamics of 5CB. Time-resolved IR data were analyzed using literature protocols[27,34] by examining the temporal evolution of a specific vibrational mode absorbance. Figure 4 shows temporal domain data for the prominent IR mode at 2226 cm^{-1} (ν_{CN}) at 25, 29, and 33 °C acquired using a 50 ms, 12 V square electric-field pulse to drive the reorganization of the equilibrium 5CB alignment. The pulse profile boundaries are depicted schematically in the figure along with data that illustrate the effects that the electrical polarizations have on the ν_{CN} optical density and thus the correlated alignment of the LC film.

One notes from Figure 4 that the electric-field-induced response of the 50-nm-thick 5CB film takes place on a several millisecond time scale. This electric-field-induced orientation response and its relaxation exhibit a striking pattern of sensitivity to temperature that is evident in terms of both impacts on band

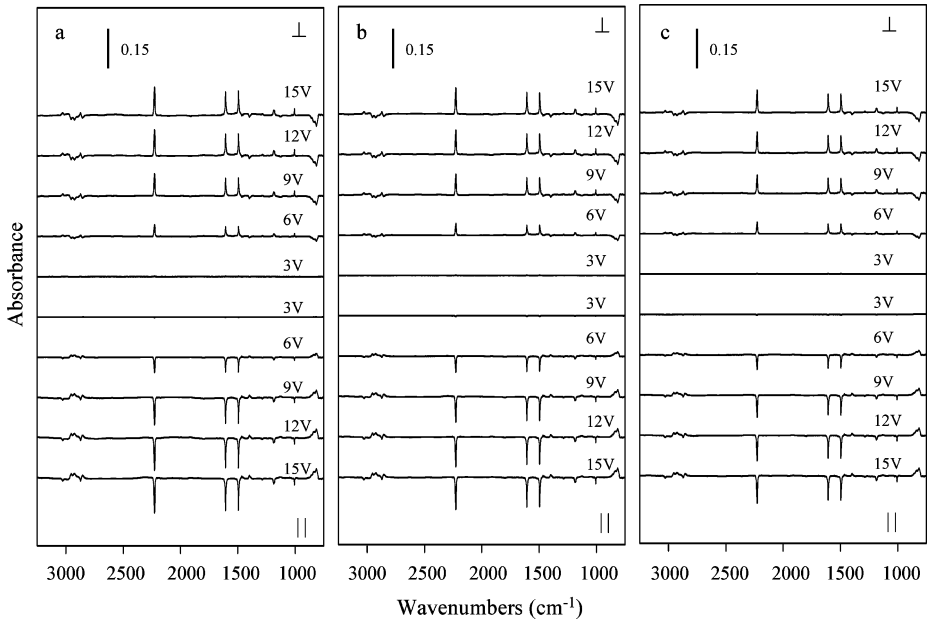

Figure 2. Static voltage spectra of the 5CB film at (a) 25, (b) 29, and (c) 33 °C. The EO cell used has a lateral electrode spacing of 15 μm. The upper panels show the data taken with perpendicular infrared polarization (parallel with the applied field), while the bottom panels show those taken with parallel polarization.

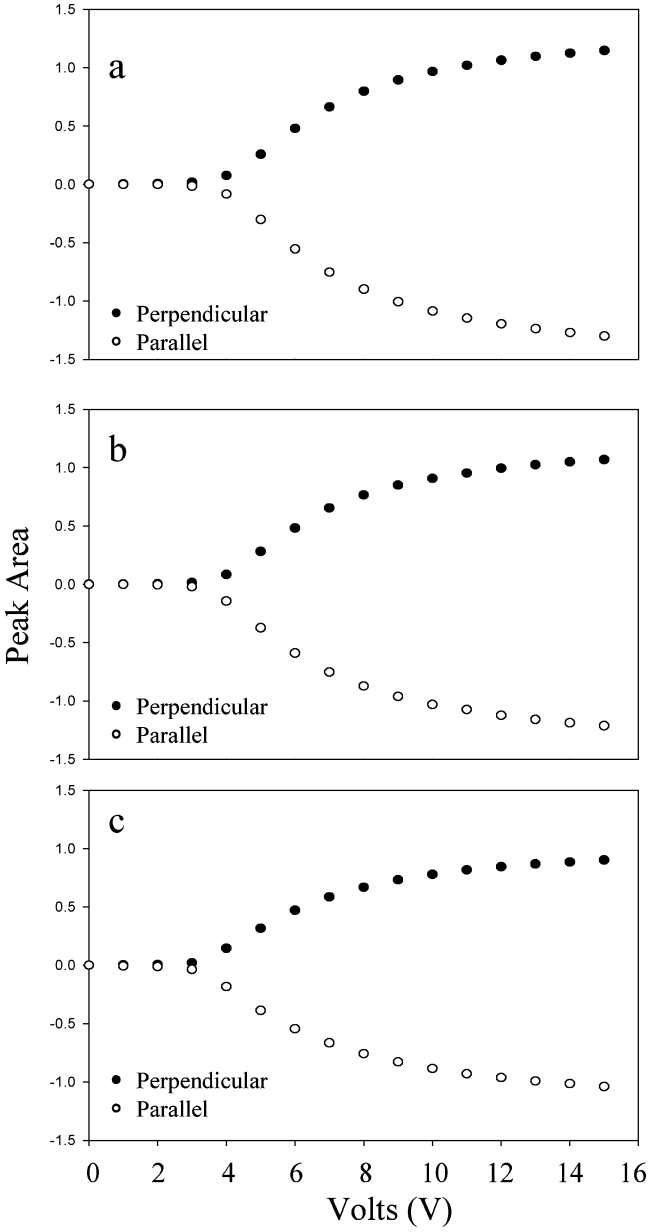

Figure 3. Integrated ν_{CN} modes plotted as a function of applied voltage at (a) 25, (b) 29, and (c) 33 °C. The EO cell used has a lateral electrode spacing of 15 μm. These data quantify the intensity differences observed in the data of Figure 2. The intensity changes indicate that the 5CB molecules orient with the field upon the application of electrical polarization.

intensity (and thus film anisotropy) and absolute rates. These issues are addressed in more detail below.

Figure 4 also shows that the absolute intensity differences measured in the perpendicular and parallel IR polarizations are not equal, a pattern that follows behaviors seen in the static voltage spectra of Figure 2. One factor contributing to these observed differences relates to the high anisotropy present in the sample.[34] In such cases, the IR intensities measured in the two polarizations of necessity will be different. This follows from the fact that the infrared intensity varies as the $\cos^2(\theta)$ (the angle, θ, is defined with respect to the electrodes) of the projection of the transition dipole moment on the polarization axis of the infrared light. For highly anisotropic media (such as is shown by data presented in Figure 1), these projections differ markedly for the two polarizations used. To eliminate errors that would result from calculating rates using data from a single polarization, we instead quantify the rate behaviors in the form

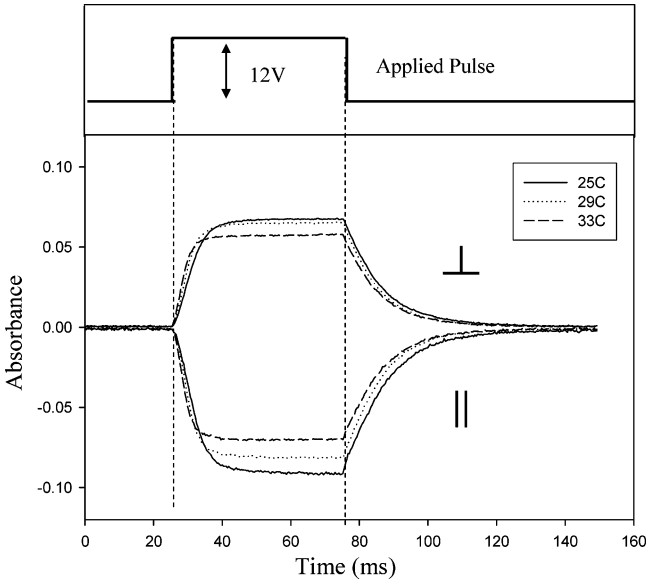

Figure 4. Temporal profiles of the TRS data in the perpendicular and parallel polarizations at 25, 29, and 33 °C. The data show the electrooptical responses of 5CB films to 12 V electric-field pulses at the ν_{CN} mode.

of the temporal evolution of the order parameter $S = (D - 1)/(D + 2)$ where D is the dichroic ratio. The method used to do this has been described in detail elsewhere.[34]

For this quantitative analysis, the orientation (the response of the LC film to the applied electric field) and the relaxation (the response when the electric field is removed) portions of the waveforms given in Figure 4 were fit with exponential regressions. The data in both cases are well described by a single-exponential formalism. Through the use of these apparent rate constants, the corrected rates are calculated, and the parameter $S_x(t)$ is calculated from the measured absorbances using the following equations[27,34]

$$S_{or} = S_{o,or} + A_{or}[1 - \exp(-k_{or}t)] \quad (1)$$

$$S_{rel} = S_{o,rel} + A_{rel}[1 - \exp(-k_{rel}t)] \quad (2)$$

where $S_x(t)$ is the time-dependent order parameter for a specific rate process, S_0 is the intercept, A is a constant, t is time, and k_{or} and k_{rel} are the orientation and relaxation rate constants, respectively. The calculated fits of $S_x(t)$ at 25, 29, and 33 °C are presented in Figure 5. The orientation order parameter decreases with applied electric field. Conversely, the relaxation profile exhibits an increase in order when the electric field is turned off and the 5CB molecules relax to their initial orientations. We further note that the explicit form of the kinetic coupling is extremely temperature-dependent; the orientation and relaxation rates soften differently with increases in temperature. We return to this point below.

The orientation and relaxation rates calculated using data taken from the ν_{CN} mode are given in Table 1. Figure 6 plots these values along with rates deduced from modes of the biphenyl moiety (modes centered at 1495 and 1607 cm^{-1}, respectively) at three temperatures. The rates found are similar irrespective of the mode used to construct the kinetic analysis. The temperature-dependent differences that exist in the orientation and relaxation rates of the LC films are apparent even from a casual inspection of the TRS profiles given in Figure 5. The orientation rate at 25 °C is the slowest, while that found at 33 °C is the fastest. The orientation rate almost doubles as the

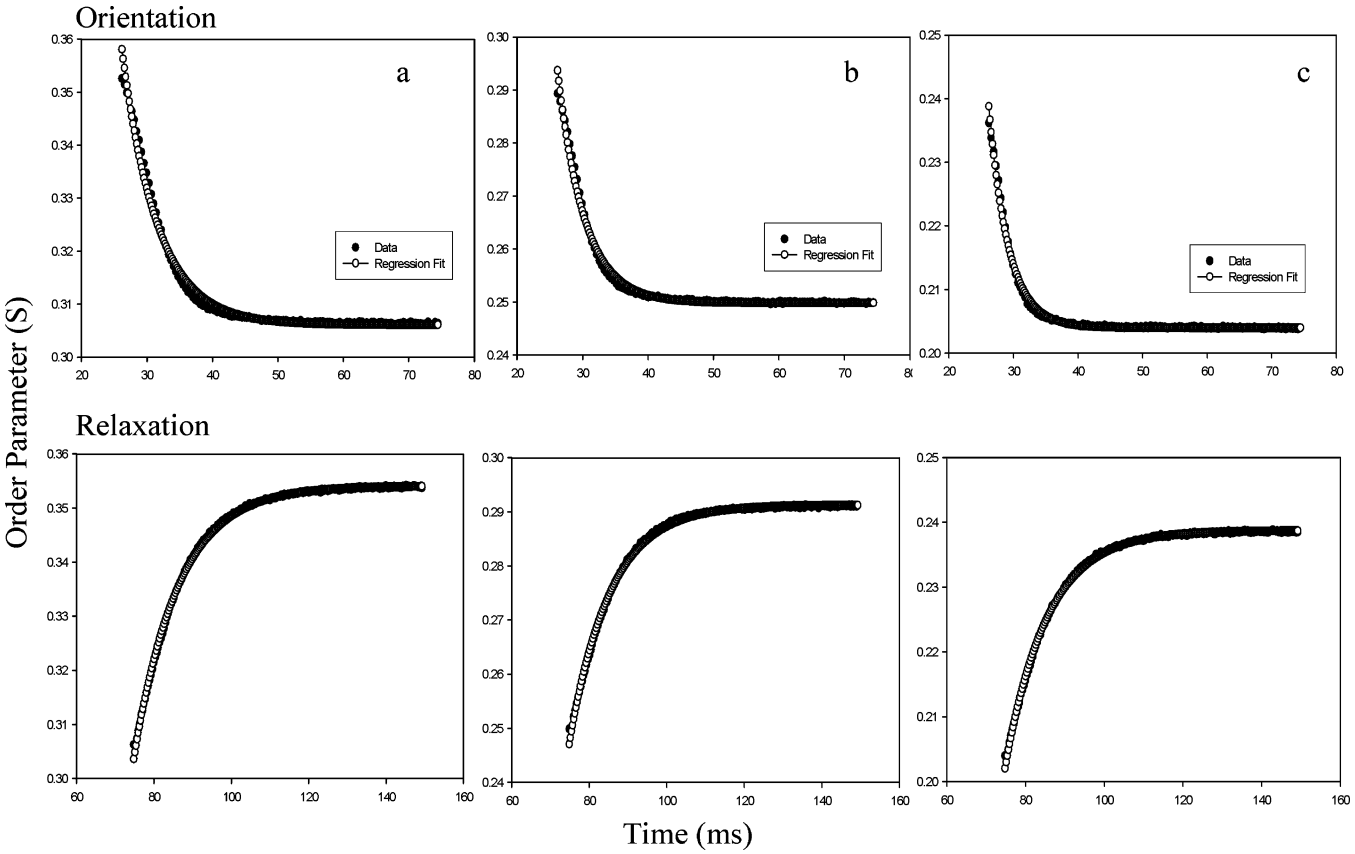

Figure 5. Top panels: Single-exponential fits of the orientation response profiles using temporal evolution of the order parameter (*S*) at (a) 25, (b) 29, and (c) 33 °C. Bottom panels: Corresponding single-exponential fits of the relaxation response profiles at these three temperatures. The negative orientation profile indicates that the order decreases as electric field is applied. (*S* is defined with respect to the parallel polarization direction.)

TABLE 1: Orientation and Relaxation Rates for the ν_{CN} Mode of 5CB, Calculated Using Order Parameters at 25, 29, and 33 °C

T (°C)	k_{or} (ms^{-1})[a]	σ (ms^{-1})[b]	k_{rel} (ms^{-1})[c]	σ (ms^{-1})[d]
25	0.1858	0.0033	0.0871	0.0004
29	0.2453	0.0041	0.0956	0.0006
33	0.3283	0.0046	0.0938	0.0004

[a] Rate constants for the orientation response of 5CB. [b] Error in fitting the orientation profile to the single-exponential form of eq 1. [c] Rate constants for the relaxation response of 5CB. [d] Error in fitting the relaxation profile to the single-exponential form of eq 2.

sample temperature is increased from 25 to 33 °C. The relaxation rates measured at these three temperatures vary to a far lesser extent than do the orientation rates. Indeed, to within experimental uncertainty k_{rel} appears to be independent of temperature. Past experiments have determined that the elastic constants[28,29,44,45] and viscosity[30,46,47] of the LC phases are temperature-dependent. Our work and that of others have also shown that these factors mediate the EO dynamics in very important ways.[29,34,45] In the subsequent sections we discuss a model that incorporates the contributions of the temperature-dependent elastic constants and viscosity to rationalize our observations.

3. Dependence of the EO Dynamics on Applied Fields. In our earlier work,[27] we reported a dependence of orientation and relaxation rates constants on the magnitude of the applied electric field. To more fully understand this phenomenon, temperature-dependent TRS experiments were carried out using square wave pulses with amplitudes ranging from 6 to 16 V. Figure 7 plots the rate constants calculated for the 50-nm-thick film at three temperatures using time-domain data extracted from the ν_{CN} stretching mode (2226 cm^{-1}). From Figure 7, a clearly

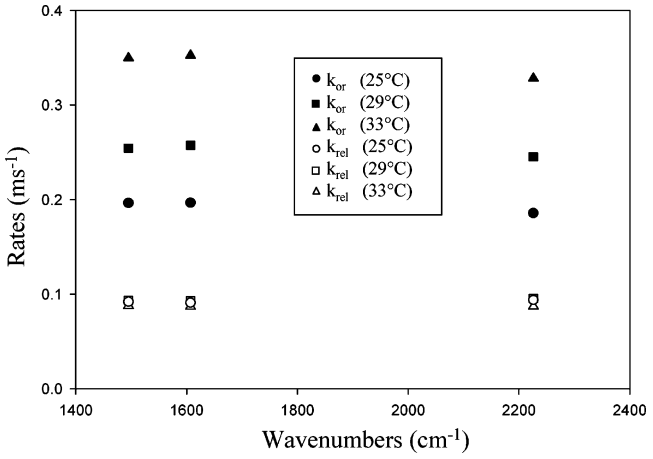

Figure 6. Comparisons of the 5CB biphenyl moiety rate constants at 25, 29, and 33 °C.

nonequivalent dependence of the orientation and relaxation rates on applied electric-field strengths is observed, which is quantitatively similar to our earlier findings.[27] A closer examination of the orientation rates suggest a parabolic dependence of these rates on the applied electric field which appears to be nearly temperature independent. The parabolic growth of the orientation rate constant with increasing applied electric-field strengths, and the approximately invariant nature of relaxation rate constants (Figure 7), appears to follow well the theoretical analysis in our earlier work based on a classic kinetic equation of motion for director dynamics.[27] The present data, however, allow us to extend our understanding of the EO dynamics of this model nanoscale system, providing an opportunity to independently assess the varying roles played by surface effects, intermolecular

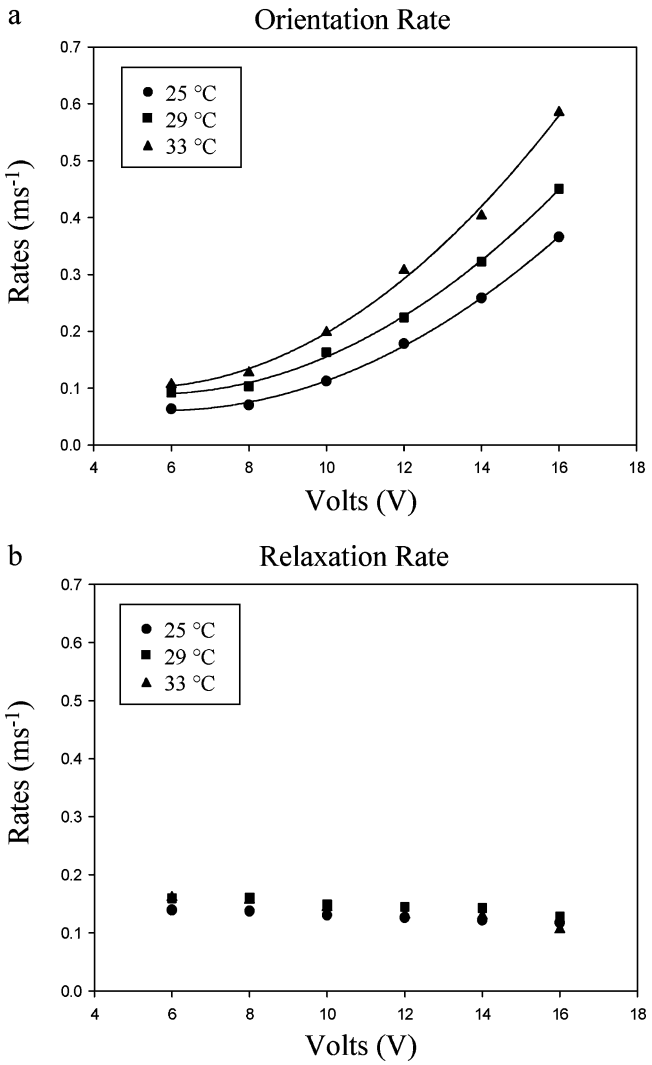

Figure 7. Temperature-dependent (a) orientation and (b) relaxation rate constants as a function of applied voltage. The rates shown are those calculated for the ν_{CN} mode at 2226 cm^{-1}. For all these films, the orientation rates increase with the application of higher fields, while the relaxation rates vary only slightly with changes in applied voltage. The trends seen in the orientation rates were best described with a quadratic regression fit.

elastic forces, and the viscous hydrodynamics of the LC medium as determinants of the EO dynamics.

A comparison made between the data obtained at 25, 29, and 33 °C makes it clear that both the surface-induced alignments and the electrooptical dynamics differ at these temperatures. It has been noted by others that the differences in alignments seen at varying temperatures can be attributed to the interplay that exists between the bulk LC−LC and the surface−LC interactions, the two having different temperature dependences.[48] On a more fundamental level, however, these differences in behavior must ultimately be related to the temperature-dependent principal elastic constants[28,29,44,45] and resultant changes in anchoring energies[49] that govern the intermolecular interactions of the liquid crystalline material. The inset in Figure 8 illustrates the nature of these temperature dependences using experimental data[44] for the splay (K_1), twist (K_2), and bend (K_3) elastic constants of 5CB along with a best fit (quadratic)[28,45] regression analysis. The data indicate that the elastic constants converge near the clearing temperature but separate as the temperature is lowered, with the bend elastic constant varying most strongly at the lower temperatures. Since these elastic constants are ones

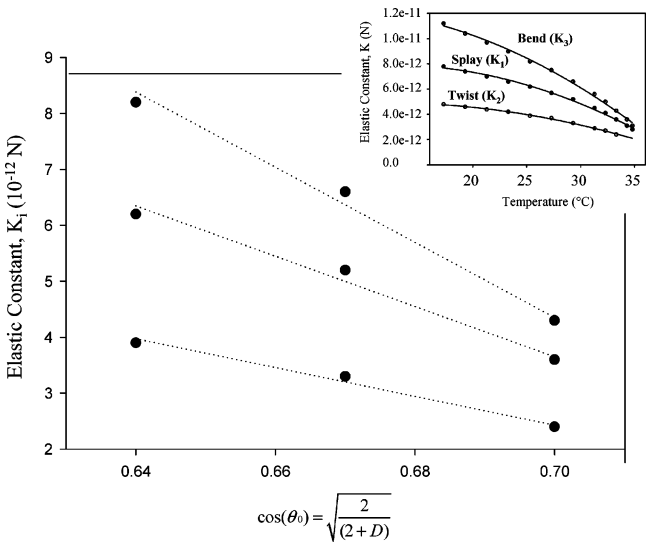

Figure 8. Temperature dependence of splay, twist, and bend elastic constants plotted as a function of $\cos(\theta_0)$ at 25, 29, and 33 °C. The plots reveal the relationship that exists between these elastic constants and the dichroisms in the LC films. Inset: Temperature dependence of the splay (K_1), twist (K_2), and bend (K_3) elastic constants. The data are taken from ref 44. All elastic constants increase in value as the temperature is lowered, but the divergence is greatest for K_3.

that mediate the EO responses, one might expect to see significant temperature scalings that follow this profile. The main part of Figure 8 demonstrates the stiffening of the elastic constants, K, upon cooling follow a linear dependence on $\cos(\theta_0) \equiv \sqrt{2/(2+D)}$, where $K = a - b\cos(\theta_0)$, a and b are positive constants, and the nematic order parameter $S = (D - 1)/(D + 2)$. The motivation for making such a plot is discussed in the next section.

Dynamical Model

The classic dynamical model employed in our previous report[27] corresponds to an overdamped kinetic equation of motion for electric-field-driven director dynamics.[28] The orientation (k_{or}) and relaxation (k_{rel}) rate constants are given by[27,28]

$$k_{rel} = \left(\frac{\pi}{d}\right)^2 \frac{K}{\eta} \tag{3}$$

$$k_{or} = k_{rel}\left[\left(\frac{V}{V_c}\right)^2 - 1\right] \tag{4}$$

$$V_c = 2\pi^{3/2}\left(\frac{K}{\Delta\epsilon}\right)^{1/2} \tag{5}$$

Here, d is the spacing between electrodes, K is the appropriate elastic constant (depending on the field-induced deformation mode), V is the applied voltage, V_c is the critical or threshold voltage required to initiate director realignment, $\Delta\epsilon$ is the difference in dielectric permittivities parallel and perpendicular to the director, and η is the relevant viscosity. According to eqs 3−5, the temperature-dependent elastic constants and viscosity affect both the orientation and the relaxation rate constants. The degree of director alignment enters implicitly. At a single fixed temperature we previously demonstrated that this simple classic model provides a good *zeroth-order* description of all the relaxation rate constant data.[27] It also rationalizes the shape of the peak area versus voltage plots, roughly the magnitude of the critical voltage and the nearly parabolic dependence of the orientational relaxation rate on applied

voltage. However, a complex dependence of the magnitude of the orientational rate constants at fixed voltage on film thickness and anchoring conditions was found that is not simply rationalizable. These strongly nonuniversal consequences of variable film thickness and surface treatment were discovered to be correlated with a specific measure of the degree of quiescent nematic order. Here we sketch the ideas developed in prior work[27] and apply and extend them to provide a physical interpretation of our new temperature-dependent data.

At high voltages well beyond the threshold value eq 4 simplifies to

$$k_{or} \cong \left(\frac{\pi}{d}\right)^2 \frac{K}{\eta}\left(\frac{V}{V_c}\right)^2 \propto \frac{\Delta\epsilon}{\eta}V^2 \tag{6}$$

The viscosity and dielectric anisotropy parameter enter the determination of k_{or} and depend on system variables including the degree of nematic order, which is highly variable depending on film thickness, surface treatment, and temperature. In reality the nematic order is described by a probability distribution due to thermal fluctuations. However, the latter are ignored in the classic mean field mesoscopic kinetic approach,[28] and one can crudely relate the orientational order parameter (S) or dichroic ratio (D) to a "mean alignment angle" $\bar{\Theta}$ as

$$S = \frac{D-1}{D+2} = \frac{3\cos^2(\bar{\Theta}) - 1}{2} \tag{7}$$

We previously argued that the electric-field-driven orientation process speeds up with decreasing nematic order.[27] One quantitative measure of the latter is the magnitude of the projection of the mean director orientation along the electric field, which is given by

$$|\sin(\bar{\Theta})| \equiv \cos(\theta_0) = \sqrt{\frac{2}{2+D}} \tag{8}$$

where $\theta_0 \equiv (\pi/2) - \bar{\Theta}$. Remarkably, at the single temperature previously studied, a (nearly) linear dependence of the orientation rate constant on $\sqrt{2/(2+D)}$ was found for all variable film thicknesses and surface treatment/anchoring conditions.[27] If interpreted in the context of the classical result of eq 6, this correlation suggests that the leading order dependence of the factor $\Delta\epsilon/\eta$ on the degree of nematic order scales as $\sqrt{2/(2+D)}$. The underlying microscopic mechanism of this remarkable correlation is not precisely established. However, one physically expects the viscous resistance for the electric-field-driven orientation orthogonal to the director will increase as the degree of quiescent nematic order increases. Equation 6 does suggest such a qualitative trend.

Comparison of Theory and Experiment

For the purposes of the discussion that follows, we consider the representative time-domain data of Figure 4. Upon application of the electrical polarizations, the prompt increase in the absorbance seen in these temporal profiles of the ν_{CN} difference spectra (Figure 4) is the result of predominantly twisting motions of the LC molecules. Our system is in some ways similar to the planar orientations examined in the earlier study.[27] One of the cells used in that study, however, was based on a somewhat different design that incorporated a polyimide planarization layer to mediate the anchoring interactions of 5CB.

Figure 9 presents our new temperature-dependent twist-dominated orientation rate constants as well as two other entries

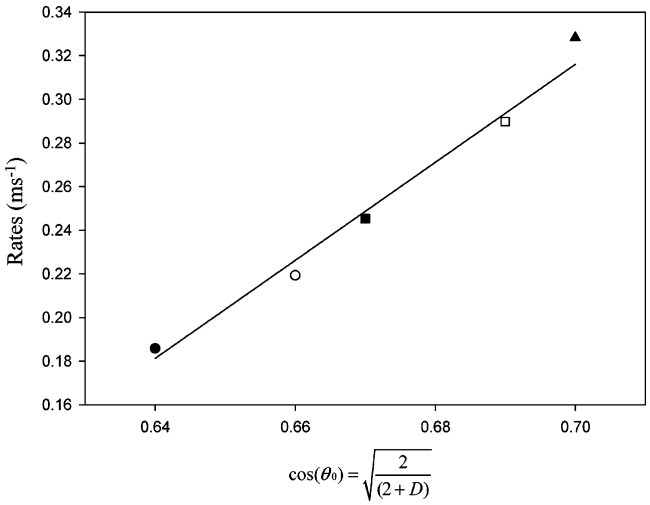

Figure 9. Orientation rate constants plotted as a function of $\cos(\theta_0) \equiv \sqrt{2/(2+D)}$; ●, ■, and ▲ represent data collected from a 50-nm-thick sample at 25, 29, and 33 °C, respectively; ○ and □ represent data collected from different 50- and 390-nm-thick samples at 25 °C, respectively, from ref 27. The data points were fit using a linear regression.

from our previous work[27] on polished ZnSe surfaces, all measured with a common applied voltage of 12 V. Motivated by the above discussion, these rate constants are plotted versus the factor $\sqrt{2/(2+D)}$. Remarkably, one notes immediately that all data points fall very nearly on a single line. This measure of the initial liquid crystalline anisotropy is temperature-dependent and appears to account for essentially all of the temperature dependence of the twist-related orientation rate constants. We should note that a similar analysis should be relevant to the thermal scalings seen in the orientation rates involving bend/splay motions, but we do not develop that here, as the anisotropy of the director in the homeotropic direction is not a parameter easily accessible to study in this EO cell geometry.

The temperature-related relationship between the LC film dichroic ratio and all three (splay, twist, and bend) elastic constants is shown in Figure 8. A striking linearity between elastic constants and $\sqrt{2/(2+D)}$ is shown. Indeed, the functional form of the relation is essentially identical for all three of the elastic constants, which increase by a common factor of $\sim 1.8 \pm 0.1$ over the range of $\sqrt{2/(2+D)}$ studied. Remarkably, the orientation rate data in Figure 9 also change by this same factor of $\sim 1.8 \pm 0.1$ over the same range of $\sqrt{2/(2+D)}$ values. Hence, the temperature dependence of k_{or} appears to follow, in an inverse manner, the elastic constants. Why might this be?

Note that the temperature dependence of the twist elastic constant (K_2) and the viscosity (η) enter in a simple way in the relaxation rates. Equation 3 predicts k_{rel} is given simply as a ratio of the latter two material parameters. One might anticipate that there would be a strong correlation between the temperature dependences of the elastic constants (as plotted in the inset of Figure 8) and the rates of the relaxation. However, the data given in Table 1 reveal that the relaxation rates change by less than 10% when the temperature is increased from 25 to 33 °C, while the elastic constant, K_2, decreases by a factor of 2 over this same range. This softening of the intermolecular elastic force that drives the system to its equilibrium configuration cannot then be solely responsible for the experimentally observed relaxation rates. As suggested by eq 3, our conclusion is that there must also be a significant, and very nearly compensating, contribution to the relaxation rate from the temperature-

dependent viscosity[7] relevant to the twist motion that will increase with cooling and enhanced nematic order.

The above analysis allows inferences to be made about the relative importance of different physical factors determining the temperature dependence of the field-induced orientation rates, k_{or}. Since k_{rel} is largely insensitive to changes in temperature, $K/\eta \approx$ constant. Hence, eq 6 suggests that the much stronger reduction of the orientation rate upon cooling at fixed voltage arises predominantly from the viscosity, which has a temperature dependence essentially identical to the elastic constant which decreases with $\sqrt{2/(2+D)}$ as seen in Figure 8. Hence, the combination of eq 6, the near temperature invariance of the relaxation rates, and the elastic constant data of Figure 8 provides a basis for understanding the remarkable correlation in Figure 9. A possible complication is the presence of the dielectric anisotropy parameter, $\Delta\epsilon$, which is also expected to be temperature-dependent. However, the fact that $\Delta\epsilon$ *increases* upon cooling but k_{or} *decreases* as the temperature is lowered, further supports our deduction that the viscosity is the dominant determining factor of the thermal dependence of the orientation rate constant.

Summarizing, for these nanoscale nematic film structures we find that temperature affects both the alignments and the electrooptical dynamics significantly. These differences depend strongly on both the temperature-dependent elastic constants and the viscosity in ways that are quantified by the temperature-dependent order parameter or dichroic ratio. The suppressed orientation rate upon cooling is deduced to be primarily controlled by the growing quiescent nematic order parameter and concomitant higher viscous resistance for rotating the director toward the (orthogonal) electric-field direction. Furthermore, for the polished cells considered here and in prior work,[27] the striking correlation shown in Figure 9 holds not only for the 50-nm-thick film but also the much thicker 390 nm film. This suggests that a remarkable simplicity exists in the sense that the consequences of a thicker film on the orientation rate constant enters solely via the modification of the nematic order parameter and its effect on the viscosity.

Conclusions

A rich temperature dependence of the electrooptical dynamics of a nematic 5CB liquid crystalline film has been observed. The experimental findings can be interpreted based on a classic coarse-grained mesoscopic model of driven director dynamics[28] discussed and applied in detail in our earlier report.[27] The electric-field-driven orientation rates were found to vary sensitively with temperature and applied voltage, while the relaxation rates do not. Furthermore, the orientation rates display a parabolic dependence on applied electric field. A linear relationship was found between a specific function of the initial anisotropy ($\sqrt{2/(2+D)}$) of the film and the measured orientation rates, which appears to *simultaneously* organize all the effects of temperature, film thickness, and surface treatment/anchoring state.

There is a caveat that merits discussion here. The present study examines a specific LC mesogen (5CB), a material that provides a model for behaviors seen in the dynamics of other nanoscale LC thin films. What implications these results hold for the more complex system used in displays remains, in some respects, an open question. The latter technologies typically exploit the properties of complex LC mixtures, which can also be formulated with specific forms of low-concentration additives (e.g., ionic compounds that act to mediate high-frequency switching behaviors). In such cases the quantitative outcomes for the dynamics, as established by the theoretical relationships employed here, need not be precisely the same. Such caution not withstanding, the present work does provide materials-based principles and device design rules that allow broad tunability of a material's dynamical responses. In future studies, we will explore these ideas in more detail, examining LC films exhibiting highly novel anisotropies and dramatically altered EO dynamics. We also intend to investigate new approaches to chemically tailor substrate surfaces to obtain anchoring interactions that can be used to embed complex hierarchical organizations into the LC mesophase. The latter work will exploit these microfabricated systems to systematically examine discrete elastic deformations occurring in complex cooperative assemblies of liquid crystalline materials.

Acknowledgment. We gratefully thank the National Science Foundation (Grant No. CHE 00-97096) and the Department of Energy (Grant No. DEFG02-91ER45439) for their support of this work. AFM studies were carried out at the Center for Microanalysis of Materials at the University of Illinois Urbana-Champaign supported by the U. S. Department of Energy under Contract No. DEFG02-91ER45439.

References and Notes

(1) Stuart, D. I.; Jones, Y. E. *Curr. Opin. Struct. Biol.* **1995**, *5*, 735.
(2) Bhushan, B.; Israelachvili, J. N.; Landman, U. *Nature* **1995**, *374*, 607.
(3) Alexopoulos, P. S.; O'Sullivan, T. C. *Annu. Rev. Mater. Sci.* **1990**, *20*, 391.
(4) Hu, Y.-Z.; Granick, S. *Tribol. Lett.* **1998**, *5*, 81.
(5) Widmer, M. R.; Heuberger, M.; Voros, J.; Spencer, N. D. *Tribol. Lett.* **2001**, *10*, 110.
(6) Kaneko, E. *Liquid Crystal TV Displays: Principles and Applications of Liquid Crystal Displays*; KTK Scientific Publishers: Tokyo, 1987.
(7) Cognard, J. *Mol. Cryst. Liq. Cryst.* **1982**, Supplement 1, 1.
(8) Jerome, B. *Rep. Prog. Phys.* **1991**, *54*, 391.
(9) (a) Maugin, C. *Compte Rendus* **1913**, *156*, 1246. (b) Maugin, C. *Bull. Soc. Fr. Mineral.* **1911**, *34*, 71. (c) Uchida, T.; Seki, H. *Surface Alignment of Liquid Crystals*; Bahadur, B., Ed.; World Scientific: Singapore, 1992.
(10) Yeh, P.; Gu, C. *Optics of Liquid Crystal Displays*; John Wiley & Sons: New York, 1999.
(11) Goossens, W. J. A. *Mol. Cryst. Liq. Cryst.* **1985**, *124*, 305.
(12) Gray, G. W.; Harrison, K. J.; Nash, J. A. *Electron. Lett.* **1973**, *9*, 130.
(13) Schadt, M. *Annu. Rev. Mater. Sci.* **1997**, *27*, 305.
(14) Bryan-Brown, G. P.; Wood, E. L.; Sage, I. C. *Nature* **1999**, *399*, 338.
(15) Clark, N. A. *Phys. Rev. Lett.* **1985**, *55*, 292.
(16) Berreman, D. W. *Phys. Rev. Lett.* **1972**, *28*, 1683.
(17) Berreman, D. W. *Mol. Cryst. Liq. Cryst.* **1973**, *23*, 215.
(18) Chaudhari, P.; Lacey, J.; Doyle, J.; Galligan, E.; Lien, S.-C. A.; Callegari, A.; Hougham, G.; Lang, N. D.; Andry, P. S.; John, R.; Yang, K.-H.; Lu, M.; Cai, C.; Speidell, J.; Purushothaman, S.; Ritsko, J.; Samant, M.; Stohr, J.; Nakagawa, Y.; Katoh, Y.; Saitoh, Y.; Sakai, K.; Satoh, H.; Odahara, S.; Nakano, H.; Nakagaki, J.; Shiota, Y. *Nature* **2001**, *411*, 56.
(19) Nejoh, H. *Surf. Sci.* **1991**, *256*, 94.
(20) Drawhorn, R. A.; Abbott, N. L. *J. Phys. Chem.* **1995**, *99*, 16511.
(21) O'Neill, M.; Kelly, S. M. *J. Phys. D: Appl. Phys.* **2000**, *33*, R67.
(22) Wu, Y.; Demachi, Y.; Tsutsumi, O.; Kanazawa, A.; Shiono, T.; Ikeda, T. *Macromolecules* **1998**, *31*, 349.
(23) Blinov, L. M.; Chigrinov, V. G. *Electrooptic Effects in Liquid Crystal Materials*; Springer-Verlag: New York, 1994.
(24) de Bleijser, J.; Leyte-Zuiderweg, L. H.; Leyte, J. C.; van Woerkom, P. C. M.; Picken, S. J. *Appl. Spectrosc.* **1996**, *50*, 167.
(25) Helfrich, W. *Mol. Cryst. Liq. Cryst.* **1973**, *21*, 187.
(26) Jones, J. C.; Worthing, P.; Bryan-Brown, G.; Wood, E. *Dig. Tech. Pap. − Soc. Inf. Disp. Int. Symp.* **2003**, *34*, 190.
(27) Lee, L. M.; Kwon, H. J.; Kang, J. H.; Nuzzo, R. G.; Schweizer, K. S. *J. Chem. Phys.* **2006**, *125*, 24705.
(28) de Gennes, P. G.; Prost, J. *The Physics of Liquid Crystals*; Oxford University Press: New York, 1993.
(29) Alexe-Ionescu, A. L.; Barbero, G.; Durand, G. *J. Phys. II* **1993**, *3*, 1247.
(30) Cui, M.; Kelly, J. R. *Mol. Cryst. Liq. Cryst.* **1999**, *331*, 49.

(31) de Jeu, W. H. *Physical Properties of Liquid Crystalline Materials*; Gordon and Breach: New York, 1980.
(32) Ashford, A.; Constant, J.; Kirton, J.; Raynes, E. P. *Electron. Lett.* **1973**, *9*, 118.
(33) Blanchard, R. M.; Noble-Luginbuhl, A. R.; Nuzzo, R. G. *Anal. Chem.* **2000**, *72*, 1365.
(34) Noble, A. R.; Kwon, H. J.; Nuzzo, R. G. *J. Am. Chem. Soc.* **2002**, *124*, 15020.
(35) Noble-Luginbuhl, A. R.; Blanchard, R. M.; Nuzzo, R. G. *J. Am. Chem. Soc.* **2000**, *122*, 3917.
(36) (a) Iimura, Y.; Akiyama, H.; Li, X. T.; Kobayashi, S. In *Photo-Alignment Control of LC and Its Applications to LCD Fabrication*; Shashidhar, R., Ed.; 1998. (b) Heckmeier, M.; Lüssem, G.; Tarumi, K.; Becker, W. *Bunsen−Magn.* **2002**, *4* (5), 106. (c) Schadt, M. *Annu. Rev. Mater. Sci.* **1997**, *27*, 305.
(37) Chatelain, P. *Bull. Soc. Fr. Mineral.* **1943**, *66*, 105.
(38) Geary, J. M.; Goodby, J. W.; Kmetz, A. R.; Patel, J. S. *J. Appl. Phys.* **1987**, *62*, 4100.
(39) Gregoriou, V. G.; Chao, J. L.; Toriumi, H.; Palmer, R. A. *Chem. Phys. Lett.* **1991**, *179*, 491.
(40) Urano, T.; Hamaguchi, H.-O. *Chem. Phys. Lett.* **1992**, *195*, 287.
(41) Hallam, B. T.; Sambles, J. R. *Liq. Cryst.* **2000**, *27*, 1207.
(42) Hiraoka, H.; Sendova, M. *Appl. Phys. Lett.* **1994**, *64*, 563.
(43) Newsome, C. J.; O'Neill, M.; Farley, R. J.; Bryan-Brown, G. P. *Appl. Phys. Lett.* **1998**, *72*, 2078.
(44) Dunmur, D. A. *Measurements of Bulk Elastic Constants of Nematics*; Dunmur, D. A., Fukuda, A., Luckhurst, G. R., Eds.; INSPEC: London, 2001.
(45) Schiele, K.; Trimper, S. *Phys. Status Solidi B* **1983**, *118*, 267.
(46) Kneppe, H.; Schneider, F.; Sharma, N. K. *J. Chem. Phys.* **1982**, *77*, 3203.
(47) Diogo, A. C.; Martins, A. F. *Mol. Cryst. Liq. Cryst.* **1981**, *66*, 133.
(48) Barbero, G.; Gabbasova, Z.; Osipov, M. A. *J. Phys. II* **1991**, *6*, 691.
(49) Blinov, L. M.; Kabayenkov, A. Y.; Sonin, A. A. *Liq. Cryst.* **1989**, *5*, 645.